Contribution from the Department of Chemistry,
State University of New York, Stony Brook, New York 11794

Kinetics and Mechanisms of the Reactions of Mononuclear and Binuclear Ruthenium(II) Ammine Complexes with Peroxydisulfate

Urs Fürholz and Albert Haim*

Received April 3, 1987

Kinetic studies of the reactions of $Ru(NH_3)_5pz^{2+}$ (pz = pyrazine), $Ru(NH_3)_4bpy^{2+}$ (bpy = 2,2′-bipyridine), $Ru(NH_3)_5pzMe^{3+}$ ($pzMe^+$ = *N*-methylpyrazinium), $Ru_2(NH_3)_{10}pz^{5+}$, $RuRh(NH_3)_{10}pz^{5+}$, and $Ru_2(NH_3)_{10}pz^{4+}$ with $S_2O_8^{2-}$ are interpreted on the basis of a mechanism involving ion-pair formation between the ruthenium complexes and $S_2O_8^{2-}$ followed by one-electron transfer from Ru(II) to $S_2O_8^{2-}$. The dependence of the rate constants upon the standard free energy changes for the above reactions as well as those of polypyridine complexes of iron(II), ruthenium(II), and osmium(II) is treated according to the Rehm–Weller mechanism and the Marcus quadratic equation that relates free energy of activation and standard free energy change. The electron-transfer step is viewed as involving the reductive cleavage of the peroxide bond in $S_2O_8^{2-}$. The reaction of $Ru_2(NH_3)_{10}pz^{4+}$ with $S_2O_8^{2-}$ yields, as kinetically controlled products, ~80% $Ru_2(NH_3)_{10}pz^{6+}$ and ~20% $Ru_2(NH_3)_{10}pz^{5+}$. The parallel formation of two- and one-electron-transfer products is interpreted on the basis of a primary one-electron-transfer mechanism to form the intimate ion pair $Ru_2(NH_3)_{10}pz^{5+}|SO_4^{-}\cdot SO_4^{2-}$ followed by competition between electron transfer within the ion pair and ion-pair separation.

The publication explosion[1] that has taken place in recent years in the area of discrete, mixed-valence complexes is characterized by an emphasis in synthetic,[2] spectroscopy,[3,4] and thermodynamic[5] aspects. In contrast, the redox reactivity of the mixed-valence binuclear complexes has been almost totally neglected. Elsewhere[6] we report reactions of (μ-pyrazine)decaammineruthenium(II,III) (hereafter, $Ru_2(NH_3)_{10}pz^{5+}$) and related complexes with several one-electron redox complexes. In the present paper, we report the reactions of $Ru_2(NH_3)_{10}pz^{4+}$, $Ru_2(NH_3)_{10}pz^{5+}$, and several mononuclear ruthenium complexes with the potentially two-electron-oxidizing agent peroxydisulfate. We address the question as to whether the reaction between $Ru_2(NH_3)_{10}pz^{4+}$ and peroxydisulfate proceeds via a one-electron or two-electron process, and we discuss the reactivity of peroxydisulfate with one-electron-reducing agents (Ru(II)–ammine complexes and polypyridine complexes of Fe(II), Ru(II), and Os(II)) in the context of the peroxide bond-breaking process and the Marcus quadratic activation free energy–standard free energy relationship.

Experimental Section

Materials. The complexes $[Ru(NH_3)_5pz](PF_6)_2$, $[Ru(NH_3)_5py](PF_6)_2$ (py is pyridine), $[Ru(NH_3)_5pzCH_3](PF_6)_3$ ($pzCH_3^+$ is *N*-methylpyrazinium), $[Ru_2(NH_3)_{10}pz](CF_3SO_3)_4$, and $[Ru_2(NH_3)_{10}pz](CF_3SO_3)_5$ were prepared as described previously.[6] Trifluoromethanesulfonic acid supplied by Alfa products was distilled twice under reduced pressure. The water used in all experiments was house-distilled water further purified by ion exchange and by distillation in an all-glass Barnstead distilling apparatus. Lithium trifluoromethanesulfonate solutions were prepared by mixing stoichiometric amounts of CF_3SO_3H and Li_2CO_3. All other chemicals were of reagent grade and were used as received.

Kinetic Measurements. All kinetic measurements were carried out in a Durrum Model D-110 stopped-flow apparatus. Absorbance vs time data were collected in a Nicolet Explorer oscilloscope interfaced with an 11V03 DEC computer. Kinetic measurements were performed at an ionic strength of 0.10 M under pseudo-first-order conditions with peroxydisulfate in at least 10-fold excess, with the exception of some of the measurements of the $Ru_2(NH_3)_{10}pz^{4+}$–$S_2O_8^{2-}$ reaction for which the reactants were in the stoichiometric (2:1 molar) ratio. Reactions were monitored at the absorbance maximum of the Ru(II) complex, and observed rate constants were calculated by means of a nonlinear least-squares fit of $A_t - A_\infty$ to t according to the equation $A_t - A_\infty = (A_0 - A_\infty)\exp(-k_{obsd}t)$.

Results

The ruthenium(III) products formed by oxidation of the ruthenium(II) reactants with peroxydisulfate are relatively unstable in neutral solution.[6] Therefore, except for $Ru(NH_3)_5pz^{2+}$, all measurements were carried out in acidic media, generally 0.050 M trifluoromethanesulfonic acid. The observed first-order rate constants at 25 °C and 0.10 M ionic strength are plotted vs the peroxydisulfate concentration in Figure 1. It will be seen that the plots are linear at low values of $[S_2O_8^{2-}]$, but that deviations from linearity obtain at higher values. The deviations are rather small for complexes of lower charge (2+), but as the charges of the complexes increase, pronounced deviations from linearity become quite apparent. These observations are accommodated on the basis of the mechanism given by eq 1–3. On the basis

$$Ru^{II}(NH_3)_5L^{n+} + S_2O_8^{2-} \rightleftharpoons Ru^{II}(NH_3)_5L^{n+}|S_2O_8^{2-} \quad \text{rapid equilibrium } Q_{IP} \quad (1)$$

$$Ru^{II}(NH_3)_5L^{n+}|S_2O_8^{2-} \rightarrow Ru^{III}(NH_3)_5L^{(n+1)+} + SO_4^{2-} + SO_4^{-} \quad \text{slow } k_{et} \quad (2)$$

$$Ru^{II}(NH_3)_5L^{n+} + SO_4^{-} \rightarrow Ru^{III}(NH_3)_5L^{(n+1)+} + SO_4^{2-} \quad \text{rapid} \quad (3)$$

of this mechanism, the rate of disappearance of the ruthenium(II) complex is given by eq 4 and k_{obsd} is given by eq 5. Values of

$$-\frac{d[Ru^{II}]}{dt} = \frac{2k_{et}Q_{IP}[S_2O_8^{2-}][Ru^{II}]}{1 + Q_{IP}[S_2O_8^{2-}]} \quad (4)$$

$$k_{obsd} = \frac{2k_{et}Q_{IP}[S_2O_8^{2-}]}{1 + Q_{IP}[S_2O_8^{2-}]} \quad (5)$$

k_{et} and Q_{IP}, obtained from the measurements by means of a nonlinear least-squares calculation, are listed in Table I (columns 2 and 3, respectively). For $Ru(NH_3)_4bpy^{2+}$, the deviations from linearity are too small. Under these circumstances, only the product $k_{et}Q_{IP}$ can be obtained from the measurements, and it is listed in column 4 of Table I. The solid lines in Figure 1 are plots of eq 5 with the parameters given in columns 2 and 3 of Table I, and it will be seen that the derived parameters reproduce the experimental results reasonably well.

Values of Q_{IP} can be estimated from eq 6–8.[7] Definitions are as follows: *N*, Avogadro's number; *a*, distance of closest approach;

$$Q_{IP} = \frac{4\pi Na^3}{3000}\exp(-U(a)/kT) \quad (6)$$

$$U(a) = \frac{Z_1Z_2e^2}{Da(1 + \kappa a)} \quad (7)$$

$$\kappa = \left(\frac{8\pi Ne^2\mu}{1000DkT}\right)^{1/2} \quad (8)$$

(1) Creutz, C. *Prog. Inorg. Chem.* **1983**, *30*, 1.
(2) Lay, P. A.; Magnuson, R. H.; Taube, H.; Ferguson, J.; Krausz, E. R. *J. Am. Chem. Soc.* **1985**, *107*, 2551.
(3) Krausz, E.; Ludi, A. *Inorg. Chem.* **1985**, *24*, 939.
(4) Dubicki, L.; Ferguson, J.; Krausz, E. R.; Lay, P. A.; Maeder, M.; Magnuson, R. H.; Taube, H. *J. Am. Chem. Soc.* **1985**, *107*, 2167.
(5) Richardson, D. E.; Taube, H. *Coord. Chem. Rev.* **1984**, *60*, 107.
(6) Fürholz, U.; Haim, A. *J. Phys. Chem.* **1986**, *90*, 3686.
(7) Miralles, A. J.; Armstrong, R. E.; Haim, A. *J. Am. Chem. Soc.* **1977**, *99*, 1416.

0020-1669/87/1326-3243$01.50/0

Table I. Rate Constants and Ion-Pair Formation Constants for Reactions of Ruthenium(II) Complexes with Peroxydisulfate at 25 °C and Ionic Strength 0.10 M[a]

complex	Q_{IP}, M^{-1}	k_{et}, s^{-1}	$Q_{IP}k_{et}$, M^{-1} s^{-1}
$Ru(NH_3)_5pz^{2+}$ [b]	14 ± 5	(2.6 ± 0.8) × 10^2	3.6 × 10^3 [c]
$Ru(NH_3)_4bpy^{2+}$ [d]	(9)[e]	(3.0 × 10^2)[f]	(2.7 ± 1) × 10^3
$Ru(NH_3)_5pzMe^{3+}$	50 ± 1	1.90 ± 0.3	9.5 × 10^c
$Ru_2(NH_3)_{10}pz^{5+}$	(2.7 ± 0.2) × 10^2	(4.7 ± 0.1) × 10	1.3 × 10^{4c}
$RuRh(NH_3)_5pz^{5+}$	(2.1 ± 0.2) × 10^2	(1.0 ± 0.1) × 10^2	2.1 × 10^{4c}
$Ru_2(NH_3)_{10}pz^{4+}$	(61)[e]	(7.1 × 10^3)[f]	4.3 × 10^5 [g]

[a] In 0.050 M CF_3SO_3H; $LiCF_3SO_3$ added as background electrolyte. [b] Unbuffered solutions at pH ~4 with $LiClO_4$ as background electrolyte. [c] Calculated from Q_{IP} and k_{et} and corrected for 3% protonation of $Ru(NH_3)_5pz^{2+}$ at pH 4; see text. [d] In 0.10 M $HClO_4$. [e] Estimated from eq 6. [f] Calculated from measured $Q_{IP}k_{et}$ and estimated Q_{IP}. [g] See text.

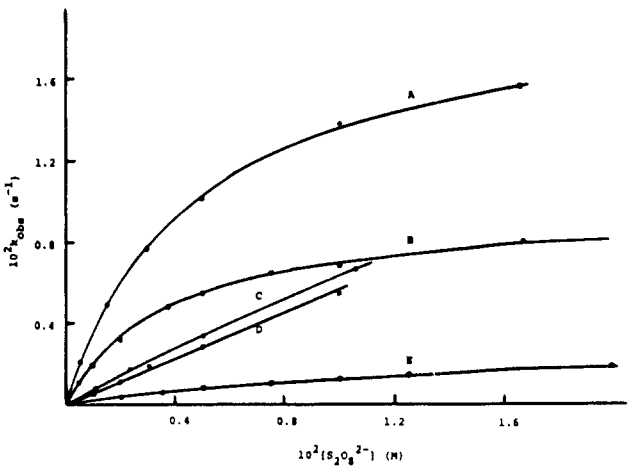

Figure 1. k_{obsd} vs concentration of peroxydisulfate for reactions of ruthenium ammine complexes: (A) $RuRh(NH_3)_{10}pz^{5+}$; (B) $Ru_2(NH_3)_{10}pz^{5+}$; (C) $Ru(NH_3)_5pz^{2+}$; (D) $Ru(NH_3)_4bpy^{2+}$; (E) $Ru(NH_3)_5pzMe^{3+}$, observed rate constant multiplied by 10.

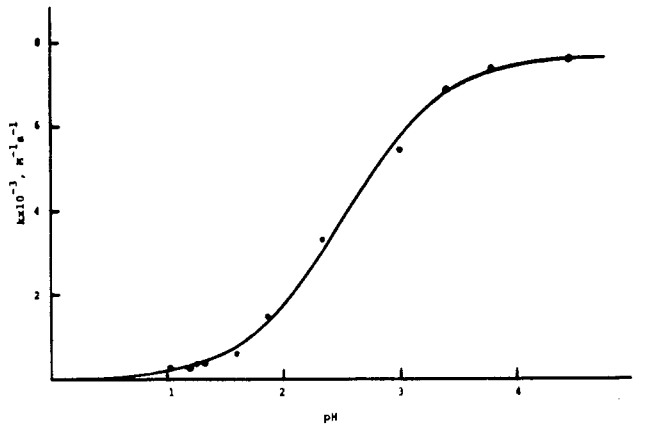

Figure 2. k for $Ru(NH_3)_5pz^{2+}$–$S_2O_8^{2-}$ reaction vs pH.

Scheme I

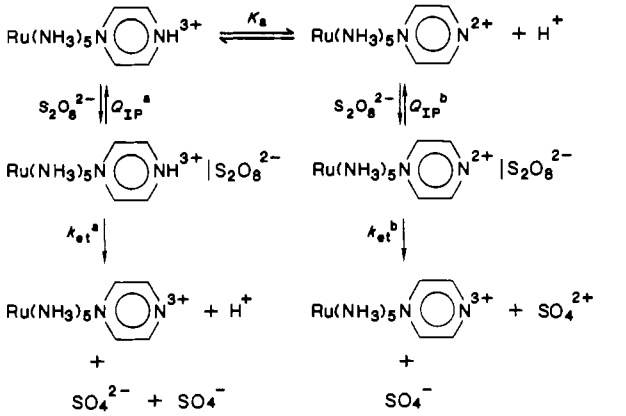

k, Boltzmann's constant; T, absolute temperature; Z_1 and Z_2, charges of ions 1 and 2, respectively; e, electronic charge; D, bulk dielectric constant; μ, ionic strength. Since the species under consideration are not spherical, values of a were estimated by adding the radii of the spheres of equal volume (3.8, 4.1, 4.7, 4.7, 3.9, and 3.4 Å for $Ru(NH_3)_5pz^{2+}$, $Ru(NH_3)_4bpy^{2+}$, $Ru_2(NH_3)_{10}pz^{5+}$, $RuRh(NH_3)_{10}pz^{5+}$, $Ru(NH_3)_5pzMe^{3+}$ and $S_2O_8^{2-}$, respectively). Estimated values of Q_{IP} for $Ru_2(NH_3)_{10}pz^{5+}$ (and $RuRh(NH_3)_{10}pz^{5+}$), $Ru(NH_3)_5pzMe^{3+}$, and $Ru(NH_3)_5pz^{2+}$, are 1.6 × 10^2, 2.8 × 10, and 9.1 M^{-1}, respectively, in good agreement with the measured values 2.7 × 10^2 (and 2.1 × 10^2), 5.0 × 10, and 14 M^{-1}. The value of Q_{IP} estimated for $Ru(NH_3)_4bpy^{2+}$ is 9.0 M^{-1} and is compatible with the observed linear dependence of k_{obsd} upon $[S_2O_8^{2-}]$ at concentrations less than 5 × 10^{-3} M and with the slight deviation from linearity at the highest concentration utilized.

The measurements of k_{obsd} for $Ru(NH_3)_5pz^{2+}$ reported in Figure 1 were carried out with unbuffered solutions at pH 4. Under these conditions, the predominant form of $Ru(NH_3)_5pz^{2+}$ (~97%) is the deprotonated form (the pK_a of the protonated form is 2.5[8]). In order to obtain the value of k_{et} and Q_{IP} for the deprotonated form from these measurements, it is necessary to ascertain the relative reactivities of protonated and deprotonated forms. This was accomplished by measuring the rate of the reaction as a function of pH. The results of these measurements are depicted in Figure 2 in the form of a plot of $k_{obsd}/[S_2O_8^{2-}]$ vs pH. The results are compatible with the mechanism given in Scheme I. According to this mechanism (with the approximation that $1 \gg Q_{IP}^{a}[S_2O_8^{2-}]$ or $Q_{IP}^{b}[S_2O_8^{2-}]$, a reasonable approximation since $[S_2O_8^{2-}] \sim 1 \times 10^{-3}$ M, $Q_{IP}^{b} \sim 9$ M^{-1} and $Q_{IP}^{a} \sim 30$ M^{-1}), k_{obsd} is given by eq 9. The measurements in Figure 2 were fitted to

$$k_{obsd} = \frac{(2k_{et}^{a}Q_{IP}^{a} + 2k_{et}^{b}Q_{IP}^{b}K_a/[H^+])[S_2O_8^{2-}]}{1 + K_a/[H^+]} \quad (9)$$

eq 9 (nonlinear least squares; k_{et}^{a} Q_{IP}^{a}, $k_{et}^{b}Q_{IP}^{b}$, and K_a taken as floating parameters). The resulting values are (in the same order) −13 ± 50 M^{-1} s^{-1}, (3.87 ± 0.33) × 10^3 M^{-1} s^{-1}, and (3.1 ± 0.3) × 10^{-3} M^{-1} (pK_a = 2.51). The value of $k_{et}^{a}Q_{IP}^{a}$ is equal to zero within experimental error. Therefore, the least-squares calculation was repeated, setting k_{et}^{a} = 0, and the resulting values of $k_{et}^{b}Q_{IP}^{b}$ and K_a were (3.85 ± 0.06) × 10^3 M^{-1} s^{-1} and (3.02 ± 0.23) × 10^{-3} M^{-1} (pK_a = 2.52 ± 0.03), respectively. The latter value is in excellent agreement with the value of 2.5 obtained from static measurements.[8] Since the protonated form of $Ru(NH_3)_5pz^{2+}$ is unreactive toward $S_2O_8^{2-}$, the measurements at pH 4 represent the reaction of the unprotonated form. In fact, the value of $k_{et}^{b}Q_{IP}^{b}$ (3.9 × 10^3 M^{-1} s^{-1}) obtained from the pH-dependent studies is in good agreement with the value calculated (3.8 × 10^3 M^{-1} s^{-1}) from the $[S_2O_8^{2-}]$-dependent measurements at pH 4 of k_{et} (2.6 × 10^2 s^{-1}, corrected to 2.7 × 10^2 s^{-1} for the 3% of unreactive protonated ruthenium complex at pH 4) and Q_{IP} (14 M^{-1}).

The studies on the oxidation of $Ru_2(NH_3)_{10}pz^{4+}$ deserve a special comment. Unlike all the other mononuclear and binuclear ruthenium(II) complexes discussed so far, the complex $Ru_2(NH_3)_{10}pz^{4+}$ is potentially capable of reducing peroxydisulfate in a single two-electron step, eq 10, or a sequence of two one-

(8) Ford, P. C.; Rudd, D. F. P.; Gaunder, R.; Taube, H. *J. Am. Chemm. Soc.* **1968**, *90*, 1187.

$$Ru_2(NH_3)_{10}pz^{4+} + S_2O_8^{2-} \rightarrow Ru_2(NH_3)_{10}pz^{6+} + 2SO_4^{2-} \quad (10)$$

electron steps, eq 11 and 12. Therefore, it is important to establish

$$Ru_2(NH_3)_{10}pz^{4+} + S_2O_8^{2-} \rightarrow Ru_2(NH_3)_{10}pz^{5+} + SO_4^{2-} + SO_4^{-} \quad (11)$$

$$Ru_2(NH_3)_{10}pz^{5+} + S_2O_8^{2-} \rightarrow Ru_2(NH_3)_{10}pz^{6+} + SO_4^{2-} + SO_4^{-} \quad (12)$$

experimentally whether we are dealing with a one-electron pathway, a two-electron pathway, or a combination of both pathways. When a $\sim 2 \times 10^{-6}$ M solution of $Ru_2(NH_3)_{10}pz^{4+}$ is oxidized with an excess of $S_2O_8^{2-}$ ($\sim 1 \times 10^{-4}$ M), the absorbance vs time traces at 550 nm (molar absorbances of $Ru_2(NH_3)_{10}pz^{4+}$, $Ru_2(NH_3)_{10}pz^{5+}$, and $Ru_2(NH_3)_{10}pz^{6+}$ are 3.0×10^4, 1.8×10^4, and 0 M^{-1} cm^{-1}, respectively) obey biphasic kinetics. The first, rapid phase (decrease in absorbance) corresponds to disappearance of $Ru_2(NH_3)_{10}pz^{4+}$ and formation of $Ru_2(NH_3)_{10}pz^{5+}$. The second, slow phase (further decrease in absorbance) corresponds to disappearance of $Ru_2(NH_3)_{10}pz^{5+}$ with concomitant formation of $Ru_2(NH_3)_{10}pz^{6+}$ (the rate constant for the second phase is in excellent agreement swith the constant measured independently for the $Ru_2(NH_3)_{10}pz^{5+}$–$S_2O_8^{2-}$ reaction). At first glance, the intermediacy of $Ru_2(NH_3)_{10}pz^{5+}$ would appear to indicate that the reaction proceeds by a mechanism that involves a sequence of one-electron steps, eq 11 and 12. However, the fact that $Ru_2(NH_3)_{10}pz^{5+}$ is kinetically detected as a transient intermediate in the reaction of $Ru_2(NH_3)_{10}pz^{4+}$ with excess $S_2O_8^{2-}$ is not proof that the reaction proceeds via two consecutive one-electron steps. To be sure, such a reaction pathway accounts for the intermediacy of $Ru_2(NH_3)_{10}pz^{5+}$. But the latter can also be formed in the two-electron pathway (eq 10) by the rapid[6] (second-order rate constant of 4.8×10^6 M^{-1} s^{-1} in 0.10 M CF_3SO_3H and $\sim 7 \times 10^7$ M^{-1} s^{-1} in 0.10 M $HClO_4$) comproportionation reaction given by eq 13. The comproportionation reaction is

$$Ru_2(NH_3)_{10}pz^{4+} + Ru_2(NH_3)_{10}pz^{6+} = 2Ru_2(NH_3)_{10}pz^{5} \quad (13)$$

important not only in the two-electron mechanism but in the one-electron mechanism as well. The complete sets of reactions for the one- and two-electron mechanisms are presented in Schemes II and III, respectively. The schemes incorporate, in addition to the reactions of $Ru_2(NH_3)_{10}pz^{4+}$ and of $Ru_2(NH_3)_{10}pz^{5+}$ with $S_2O_8^{2-}$ (eq 11 and 12) and the comproportionation reaction (eq 13), the reactions of $Ru_2(NH_3)_{10}pz^{4+}$ and of $Ru_2(NH_3)_{10}pz^{5+}$ with SO_4^- radicals (eq 14 and 15). Before describing the experiments that were performed in order to distinguish between the one- and two-electron mechanisms, it is instructive to compare Schemes II and III. Although four (eq 12–15) of the five reactions are common to both mechanisms, the initial step in each sequence differs, being either a one-electron (Scheme II) or a two-electron (Scheme III) reaction. The corresponding primary reaction products are also different, namely, $Ru_2(NH_3)_{10}pz^{6+}$ for the one-electron and two-electron mechanisms, respectively. Consequently, during the initial stages of the reaction, when the concentration of the primary reaction product is small, reactions 12, 13, and 15 are negligible, the one-electron mechanism reduces to eq 11 and 14, and the two-electron mechanism reduces to eq 10. The corresponding stoichiometries are 2 mol of $Ru_2(NH_3)_{10}pz^{4+}$ consumed and 2 mol of $Ru_2(NH_3)_{10}pz^{5+}$ produced per 1 mol of $S_2O_8^{2-}$ consumed, and 1 mol of $Ru_2(NH_3)_{10}pz^{4+}$ consumed and 1 mol of $Ru_2(NH_3)_{10}pz^{6+}$ produced per 1 mol of $S_2O_8^{2-}$ consumed for the one-electron and two-electron mechanisms, respectively. Moreover, it will be seen that the two mechanisms differ with respect to the effect of SO_4^- radical scavengers on the reaction rate. During the initial stages of the reaction, the rate of disappearance of $Ru_2(NH_3)_{10}pz^{4+}$ would be unaffected by radical scavengers in the two-electron mechanism, whereas the rate would be decreased by a factor of 2 in the one-electron mechanism. These differences were exploited in experiments designed to distinguish between the one- and two-electron mechanisms, and such experiments are described in detail now.

Scheme II. One-Electron Mechanism

$$Ru_2(NH_3)_{10}pz^{4+} + S_2O_8^{2-} \xrightarrow{k_{11}} Ru_2(NH_3)_{10}pz^{5+} + SO_4^{2-} + SO_4^{-} \quad (11)$$

$$Ru_2(NH_3)_{10}pz^{5+} + S_2O_8^{2-} \rightarrow Ru_2(NH_3)_{10}pz^{6+} + SO_4^{2-} + SO_4^{-} \quad (12)$$

$$Ru_2(NH_3)_{10}pz^{4+} + Ru_2(NH_3)_{10}pz^{6+} \rightarrow 2Ru_2(NH_3)_{10}pz^{5+} \quad (13)$$

$$Ru_2(NH_3)_{10}pz^{4+} + SO_4^{-} \rightarrow Ru_2(NH_3)_{10}pz^{5+} + SO_4^{2-} \quad (14)$$

$$Ru_2(NH_3)_{10}pz^{5+} + SO_4^{-} \rightarrow Ru_2(NH_3)_{10}pz^{6+} + SO_4^{2-} \quad (15)$$

Scheme III. Two-Electron Mechanism

$$Ru_2(NH_3)_{10}pz^{4+} + S_2O_8^{2-} \xrightarrow{k_{10}} Ru_2(NH_3)_{10}pz^{6+} + 2SO_4^{2-} \quad (10)$$

$$Ru_2(NH_3)_{10}pz^{4+} + Ru_2(NH_3)_{10}pz^{6+} \rightarrow 2Ru_2(NH_3)_{10}pz^{5+} \quad (13)$$

$$Ru_2(NH_3)_{10}pz^{5+} + S_2O_8^{2-} \rightarrow Ru_2(NH_3)_{10}pz^{6+} + SO_4^{2-} + SO_4^{-} \quad (12)$$

$$Ru_2(NH_3)_{10}pz^{4+} + SO_4^{-} \rightarrow Ru_2(NH_3)_{10}pz^{5+} + SO_4^{2-} \quad (14)$$

$$Ru_2(NH_3)_{10}pz^{5+} + SO_4^{-} \rightarrow Ru_2(NH_3)_{10}pz^{6+} + SO_4^{2-} \quad (15)$$

Several types of experiments were performed. The first set of experiments, designed to obtain an accurate measurement of the rate constant for the reaction, was carried out at low, stoichiometric reactant concentrations ($[Ru_2(NH_3)_{10}pz^{4+}] = 2[S_2O_8^{2-}]$). Under these conditions, the reaction obeys second-order kinetics, the reaction stoichiometry is given by eq 16, and the comproportionation reaction (eq 10) is fast compared to the $Ru_2(NH_3)_{10}pz^{4+}$–$S_2O_8^{2-}$ or $Ru_2(NH_3)_{10}pz^{5+}$–$S_2O_8^{2-}$ reactions. Under these conditions, the functional dependence of the absorbance (A_t) with respect to time (t) is given by eq 17, where A_0 and A_∞ are

$$2Ru_2(NH_3)_{10}pz^{4+} + S_2O_8^{2-} = 2Ru_2(NH_3)_{10}pz^{5+} + 2SO_4^{2-} \quad (16)$$

$$A_t = A_\infty + \frac{A_0 - A_\infty}{1 + [Ru_2(NH_3)_{10}pz^{4+}]_0 kt} \quad (17)$$

the absorbance at time 0 and at the end of the reaction, respectively, and k is the observed second-order rate constant. Measurements at 25 °C with $[Ru_2(NH_3)_{10}pz^{4+}] = 2 \times 10^{-6}$ to 1×10^{-5} M and $[S_2O_8^{2-}] = 1 \times 10^{-6}$ to 5×10^{-6} M yielded values of k equal to $(3.9 \pm 0.2) \times 10^5$ M^{-1} s^{-1} in 0.050 M $HClO_4$/0.05 M $LiClO_4$ and $(8.6 \pm 0.3) \times 10^5$ M^{-1} s^{-1} in 0.050 M HCF_3SO_3/0.050 M $LiCF_3SO_3$. The observed rate constant k is k_{11}, k_{10}, or $k_{11} + k_{10}$ depending on whether a one-electron, a two-electron, or a parallel one- and two-electron mechanism obtains. The second set of experiments was designed to distinguish between the one- and two-electron mechanisms by comparing the observed absorbance at 550 nm vs time variation with that expected for Scheme II or Scheme III. Here an excess of $S_2O_8^{2-}$ over $Ru_2(NH_3)_{10}pz^{4+}$ was utilized (5.0×10^{-5} M and 1.86×10^{-6} M, respectively). The absorbances at 550 nm were calculated[9] for Scheme II and for Scheme III and are depicted in Figure 3 as curves A and C, respectively. Although the measurements were not restricted to the initial stages of the reaction, the trends discussed above are clearly discernible. In the one-electron mechanism (curve A) the absorbance change corresponds qualitatively to the transformation $Ru_2(NH_3)_{10}pz^{4+}$ to $Ru_2(NH_3)_{10}pz^{5+}$, whereas for the two-electron mechanism (curve B),

(9) The systems of stiff differential equations resulting from Schemes II and III were solved by utilizing a modification (Gear's) of the 1980 version of the Lawrence Livermore solver of ordinary differential equations. Values of the rate constants were k_{11} or $k_{15} = 8.6 \times 10^5$ M^{-1} s^{-1}, $k_{12} = 1.25 \times 10^4$ M^{-1} s^{-1}, $k_{13} = k_{14} = 4 \times 10^9$ M^{-1} s^{-1}, and $k_{10} = 4.8 \times 10^6$ M^{-1} s^{-1}.

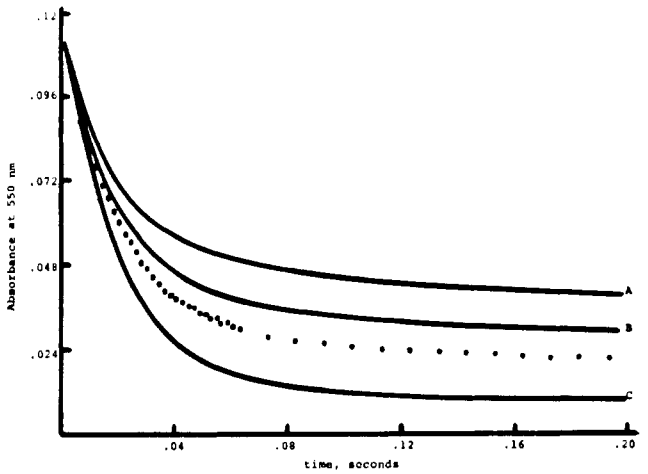

Figure 3. Absorbance at 550 nm vs time for reaction of $S_2O_8^{2-}$ (5.0×10^{-5} M) with $Ru_2(NH_3)_{10}pz^{4+}$ (1.86×10^{-6} M) at 25 °C, 0.10 M CF_3SO_3H, 2-cm cell. Points are experimental values. Solid lines are (A) 100% one-electron pathway, (B) 50% each one-electron and two-electron pathways, and (C) 100% two-electron pathway.

the absorbance change corresponds qualitatively to the transformation $Ru_2(NH_3)_{10}pz^{4+}$ to $Ru_2(NH_3)_{10}pz^{6+}$. The observed points are also displayed in Figure 3 as is the calculated absorbance (curve B) for equal contributions of the one- and two-electron mechanisms. It will be seen that the observed points indicate that more than half of the reaction proceeds via the two-electron mechanism. By calculating the absorbance vs time curves for several ratios of the one- and two-electron pathways and comparing the resulting curves with the experimental points, we estimate that 78 ± 5% of the reaction proceeds by the two-electron mechanism. In the third set of experiments, again conducted in order to distinguish between the one- and two-electron mechanisms, scavenging of the SO_4^- radicals was sought. To be sure, the requirements for a suitable scavenger are very stringent: its reduced form may only react with SO_4^- (no reaction with $S_2O_8^{2-}$, $Ru_2(NH_3)_{10}pz^{5+}$, or $Ru_2(NH_3)_{10}pz^{6+}$) and its oxidized form may not react with any reducing species present in the system ($Ru_2(NH_3)_{10}^{4+}$ or $Ru_2(NH_3)_{10}pz^{5+}$). Of all the species that we tried—acrylamide, triethanolamine, iodide, thiocyanate, and iron(II)—only the latter meets approximately the requirements stipulated above. The measurements were carried out under stoichiometric conditions, e.g., two $[S_2O_8^{2-}]$ to one $[Ru_2(NH_3)_{10}pz^{4+}]$, and two pieces of information were obtained from each kinetic run, namely, the total absorbance change, $A_0 - A_\infty$, upon reaction and the second-order rate constant. The results are presented in Table II, and it will be seen that the absorbance change decreases with increasing Fe(II) concentration whereas the rate constant remains constant or increases with increasing Fe(II) concentration. In the presence of Fe(II), in addition to the reactions included in Schemes II or III, the following reactions must be considered:

$$Fe^{2+} + S_2O_8^{2-} \rightarrow Fe^{3+} + SO_4^{2-} + SO_4^- \quad (18)$$

$$Fe^{2+} + SO_4^- \rightarrow Fe^{3+} + SO_4^{2-} \quad (19)$$

$$Fe^{2+} + Ru_2(NH_3)_{10}pz^{6+} \rightarrow Fe^{3+} + Ru_2(NH_3)_{10}pz^{5+} \quad (20)$$

$$Fe^{3+} + Ru_2(NH_3)_{10}pz^{4+} \rightarrow Fe^{2+} + Ru_2(NH_3)_{10}pz^{5+} \quad (21)$$

Cursory studies of reactions 18, 20, and 21 were carried out to obtain estimates of the corresponding rate constants. The values obtained (25 °C, ionic strength 0.10 M, trifluoromethanesulfonate) were $k_{18} = 26\ M^{-1}\ s^{-1}$, $k_{20} = 28\ M^{-1}\ s^{-1}$, $k_{-20} = 6.1\ M^{-1}\ s^{-1}$, $k_{21} = 2.4 \times 10^{-3}\ M^{-1}\ s^{-1}$, and $k_{-21} = 1.5 \times 10^{-3}\ M^{-1}\ s^{-1}$. The rate constant for reaction 19, $k_{19} = 8.8 \times 10^8\ M^{-1}\ s^{-1}$, has been measured previously.[10] The systems of differential equations derived from eq 11–15 and 18–21 (one-electron mechanism) and from eq 10, 12–15, and 18–21 (two-electron mechanism) were integrated numerically,[9] and the absorbance at 550 nm was calculated as a function of time. The absorbance vs time values were fitted to eq 17 (A_0, A_∞, and k were floated) and the resulting values of $A_0 - A_\infty$ and of k are also included in Table II. It will be seen that the one- and two-electron mechanisms display different trends. For the one-electron mechanism, both $A_0 - A_\infty$ and k decrease considerably with increasing Fe(II) concentration. In contrast, for the two-electron mechanism $A_0 - A_\infty$ decreases slightly and k increases slightly with increasing Fe(II) concentration. By comparing the experimental results with those anticipated for the one- or two-electron mechanisms, we estimate that the reaction proceeds by both one- and two-electron mechanisms, with the contribution of the latter being about 70 ± 10%. Finally, initial slopes under nearly stoichiometric conditions in the presence and absence of Fe(II) were measured. According to Scheme III and eq 18–21, the initial slope should be unaffected by the addition of Fe(II).[11] In contrast, for Scheme II and eq 18–21, the initial rate should decrease by a factor of 2 when sufficient Fe(II) is added to scavenge all the SO_4^- generated in the system.[11] The measurements were carried out with $[Ru_2(NH_3)_{10}pz^{4+}] = 1.46 \times 10^{-5}$ M and $[S_2O_8^{2-}] = 5 \times 10^{-6}$ M, at 25 °C and ionic strength 0.10 M (0.05 M $HClO_4$–0.05 M $LiClO_4$). The rate constants obtained from the measured initial rates at 0 and 1.0×10^{-3} M Fe(II) were 3.3×10^5 and $3.5 \times 10^5\ M^{-1}\ s^{-1}$, respectively. On the basis of the decrease in rate, we estimate an 88 ± 5% contribution of the two-electron pathway. Combining the three sets of measurements designed to answer the question of the one- vs the two-electron mechanism, we estimate that 80 ± 10% of the $Ru_2(NH_3)_{10}pz^{4+}$–$S_2O_8^{2-}$ reaction proceeds via the two-electron pathway, the balance representing the contribution of the one-electron pathway.

Table II. Absorbance Changes and Rate Constants for the $Ru_2(NH_3)_{10}pz^{4+}$–$S_2O_8^{2-}$ Reaction[a]

$[Fe^{2+}]$, M	$(A_0 - A_\infty)_{exptl}$[b]	$10^{-5}k_{exptl}$,[b] $M^{-1}\ s^{-1}$	$(A_0 - A_\infty)_{sim}$[c]	$10^{-5}k_{sim}$,[c] $M^{-1}\ s^{-1}$
0	0.133	3.7	0.122, 0.118	3.63, 3.88
1.0×10^{-5}	0.122	3.7	0.108, 0.118	3.51, 3.90
1.0×10^{-4}	0.122	3.4	0.082, 0.117	3.36, 3.95
1.0×10^{-3}	0.108	4.1	0.076, 0.116	2.95, 4.00

[a] At 25 °C, 0.050 M $HClO_4$, ionic strength 0.10 M maintained with $LiClO_4$, $[Ru_2(NH_3)_{10}pz^{4+}] = 1.0 \times 10^{-5}$ M, $[S_2O_8^{2-}] = 5.0 \times 10^{-6}$ M. [b] From fitted values of A_0, A_∞, and k obtained by nonlinear least-squares treatment of experimental A_t vs t data according to eq 17. [c] Numerical integration of Scheme II and eq 18–21 or Scheme III and eq 18–21 yielded values of A_t vs t that were fitted to eq 17 to obtain values of $(A_0 - A_\infty)_{sim}$ and k_{sim}. First and second entries correspond to one- and two-electron mechanisms, respectively.

Discussion

In several studies[12-15] of the oxidation of polypyridine complexes of iron(II), ruthenium(II), and osmium(II) by peroxydisulfate, it has been found that a linear free energy relationship is obeyed; e.g., the logarithm of the second-order rate constant for the reaction decreases linearly with an increase in the reduction potential of the M(III)/M(II) couple. The slopes of such linear plots fall[12-15] in the range −5 to −7 V^{-1} (corresponding to −0.3 to −0.4 in the free energy of activation vs. standard free energy plots). A mechanistic interpretation of these results will be presented below. However, at the outset, it must be emphasized that the linear relationship is obeyed, in part, because all of the complexes

(10) Heckel, E.; Henglein, A.; Beck, G. *Ber. Bunsen-Ges. Phys. Chem.* **1966**, *70*, 149.

(11) Numerical integration of the differential equations derived from Scheme III and eq 18–21 yields identical initial rates, which correspond to a second-order rate constant of $3.9 \times 10^5\ M^{-1}\ s^{-1}$. For Scheme II and eq 18–21, initial rates in the absence and in the presence of 1.0×10^{-3} M Fe(II) correspond to rate constants of 3.7×10^5 and $1.85 \times 10^5\ M^{-1}\ s^{-1}$, respectively.

(12) Irvine, D. H. *J. Chem. Soc.* **1959**, 2977.

(13) Burgess, J.; Prince, R. H. *J. Chem. Soc. A* **1966**, 1772.

(14) Raman, S.; Brubaker, C. H. *J. Inorg. Nucl. Chem.* **1969**, *31*, 1091.

(15) Burgess, J.; Prince, R. H. *J. Chem. Soc. A* **1970**, 2111.

studied have the same charge and similar rate constants for self-exchange.

For the reactions studied in the present work, it will be seen that the second-order rate constants do not vary monotonically with the reduction potentials of the Ru(III)/Ru(II) couples. This is not unexpected since the charges of the complexes cover the range +2 to +5 and the self-exchange rates vary by 3 orders of magnitude.[6] On the other hand, the first-order ate constants for internal electron transfer within the ion pairs do conform to a reasonable linear relationship between log k_{et} and $E°$ with a slope of -6 V^{-1} (0.36 in the corresponding free energy plot).

Linear free energy relationships of slope near 0.5 in the mildly exoergonic regime have been found for transition-metal-complex outer-sphere reactions that obey the Marcus–Hush theory of adiabatic electron transfer.[16] However, it must be noted that the peroxydisulfate reactions with transition-metal complexes are not simple one-electron-transfer reactions but rather involve the reductive cleavage of the peroxide bond and generation of the sulfate radical ion.[17] Other reductive cleavage reactions, namely, those of peroxides and organic halides, have received considerable attention in recent years and have been found to obey linear free energy relationships with slopes somewhat less than 0.5.[18-21] Various treatments[18-22] have been proposed to correlate the rates of reductive cleavage reactions with the thermodynamic strengths of the reductants. All of the approaches involve the diffusion-controlled formation of an encounter complex followed by electron transfer within the encounter complex. The dependence of the rate upon the standard free energy change for the electron-transfer step is taken to be given either by the Marcus quadratic expression[19-21] or by an empirical[22] equation. We choose to treat the reductive cleavage reactions of peroxydisulfate by utilizing the Rehm–Weller mechanism[18,23] and the Marcus free energy dependence.[16,19,20] This is basically the approach suggested by Scandola, Balzani, and Schuster[22] modified by utilizing the Marcus quadratic expression rather than the empirical dependence chosen by the latter authors. It is also the approach utilized previously[24] to correlate outer-sphere reactions of the Fe^{2+}/Fe^{3+} couple with a variety of one-electron redox transition-metal complexes. The approach is applicable to both reversible and irreversible electron-transfer processes[22] and accounts for slopes of 0.5 when $\Delta G°$ is near 0 and for slopes somewhat smaller than 0.5 in the more exoergonic regime.

The Rehm–Weller mechanism adapted to the reduction of peroxydisulfate by transition-metal complexes is depicted in eq 22. Although the present work provides kinetic evidence for the

$$M + S_2O_8^{2-} \underset{k_{21}}{\overset{k_{12}}{\rightleftharpoons}} M|S_2O_8^{2-} \underset{k_{32}}{\overset{k_{23}}{\rightleftharpoons}} M^+|SO_4^-\cdot SO_4^{2-} \xrightarrow{k_{30}} M^+ + SO_4^{2-} + SO_4^- \quad (22)$$

presence of the ion pair $M|S_2O_8^{2-}$ at detectable concentrations, this result does not prove that the ion pair is reactive. However, for simplicity it will be assumed that the ion pair is, in fact, an intermediate along the pathway to products. Moreover, it is assumed that the potential energy surface for $S_2O_8^{3-}$, the one-electron-reduction product of $S_2O_8^{2-}$ is dissociative along the O–O coordinate and that the reduction produces an intimate ion pair between $SO_4^{2-} + SO_4^-$. Although the formal O–O bond order

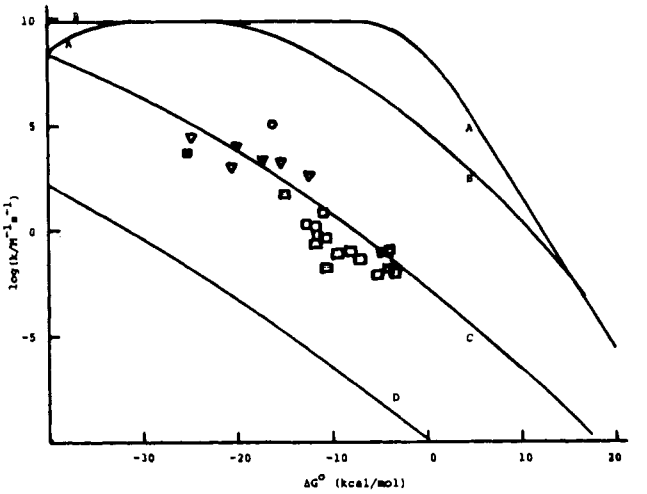

Figure 4. log k vs. $\Delta G°$ for reductive cleavage of $S_2O_8^{2-}$: (□) polypyridine complexes of Fe(II), Ru(II), and Os(II); (△) ammine complexes of Ru(II); (■) $Co(bpy)_3^{2+}$; (○) Fe^{2+}. Solid lines A–D were calculated with $\Delta G^*(0)$ = 5, 10, 20, and 30 kcal/mol, respectively.

in the hypothetical species $S_2O_8^{3-}$ is $^1/_2$, it is reasonable to assume on the basis of the concentration of negative charge and the weakness[17] of the O–O bond in $S_2O_8^{2-}$ that reduction of $S_2O_8^{2-}$ is concomitant with bond cleavage. On the basis of eq 22 and with application of the steady-state approximation to the intermediates $M|S_2O_8^{2-}$ and $M^+|SO_4^{2-}\cdot SO_4^-$, the second-order rate constant for the $M-S_2O_8^{2-}$ reaction is given by eq 23. The rate

$$k_{obsd} = \frac{k_{12}}{1 + \frac{k_{21}}{k_{23}} + \frac{k_{32}k_{21}}{k_{23}k_{30}}} \quad (23)$$

constant k_{23} for internal electron transfer within the ion pair is given by eq 24, where Z is taken to be 10^{11} M^{-1} s^{-1}. Finally, the

$$k_{23} = Ze^{-\Delta G^*/RT} \quad (24)$$

Marcus quadratic equation, eq 25, describes the relationship

$$\Delta G^* = (\Delta G^*(0))\left(1 + \frac{\Delta G_{23}°}{4\Delta G^*(0)}\right)^2 \quad (25)$$

between the free energy of activation ΔG^* and the standard free energy change $\Delta G_{23}°$ for the electron-transfer step and the intrinsic barrier $\Delta G^*(0)$, e.g., the free energy of activation when $\Delta G_{23}°$ = 0. Combination of eq 23 and 24 yields eq 26. Values of k_{12},

$$k_{obsd} = k_{12}/\left(1 + \frac{k_{21}}{Z}e^{\Delta G^*/RT} + \frac{k_{21}}{k_{30}}e^{\Delta G_{23}°/RT}\right) \quad (26)$$

k_{21}, and k_{30} for M = $Fe(bpy)_3^{2+}$ were estimated from equations for diffusion and for ion-pair formation constants and yielded the values $k_{12} = 8 \times 10^9$ M^{-1} s^{-1}, $k_{21}/Z = 7 \times 10^{-3}$ and k_{21}/k_{30} = 7 (25 °C and ionic strength 0.10 M). Figure 4 displays plots of log k_{obsd} vs. $\Delta G_{23}°$ obtained by using the above parameters and $\Delta G^*(0)$ values of 5, 10, 20, and 30 kcal/mol. It will be seen that the curves are very similar to those calculated by Scandola, Balzani, and Schuster,[22] who utilized an empirical dependence of ΔG^* upon $\Delta G_{23}°$. In particular, it must be noted that the instantaneous slopes of the log k vs $\Delta G_{23}°$ plots are $-1/4.6RT$ = −0.37 (corresponding to −0.5 in the ΔG^* vs. $\Delta G_{23}°$ plots) when $\Delta G_{23}°$ = 0, and decrease as $\Delta G_{23}°$ becomes more negative. For high values of $\Delta G^*(0)$ (20–30 kcal/mol) and relatively narrow ranges of $\Delta G_{23}°$ values (0 to −20 kcal/mol), the curves can be approximated by reasonable straight lines of slopes −0.31 (corresponding to −0.4 in the ΔG^* vs. $\Delta G_{23}°$ plots). Included in Figure 4 are the experimental points (squares) for iron, ruthenium, and osmium polypyridine complexes. Values of $\Delta G_{23}°$ were obtained from the known reduction potential of the metal complex couple and the value 1.39 V for the $S_2O_8^{2-}/SO_4^-\cdot SO_4^{2-}$ couple. The latter

(16) Sutin, N. *Prog. Inorg. Chem.* **1983**, *30*, 441.
(17) Wilmarth, W. K.; Haim, A. In *Peroxide Reaction Mechanisms*; Edwards, J. O., Ed. Interscience: New York, 1961.
(18) Schuster, J. B. *J. Am. Chem. Soc.* **1979**, *101*, 5851.
(19) Eberson, L. *Acta Chem. Scand., Ser. B* **1982**, *B36*, 533.
(20) Andrieux, C. P.; Gallardo, I.; Saveant, J. M.; Su, K. B. *J. Am. Chem. Soc.* **1986**, *108*, 638.
(21) Andrieux, C. P.; Saveant, J. M.; Su, K. B. *J. Phys. Chem.* **1986**, *90*, 3815.
(22) Scandola, F.; Balzani, V.; Schuster, G. B. *J. Am. Chem. Soc.* **1981**, *103*, 2519.
(23) Rehm, D.; Weller, A. *Isr. J. Chem.* **1970**, *8*, 259.
(24) Fürholz, U.; Haim, A. *Inorg. Chem.* **1985**, *24*, 3091.
(25) Schwarz, H. A.; Dodson, R. W. *J. Phys. Chem.* **1984**, *88*, 3643.
(26) Klaning, U. K.; Schested, K.; Holeman, J. *J. Phys. Chem.* **1985**, *89*, 760.
(27) Latimer, W. M. *Oxidation Potentials*; Prentice-Hall: New York, 1952.

value was estimated by combining the values $K \sim 10^3$ M^{-2},[17] −2.73 V,[25,26] 2.01 V,[27] and $K \sim 5 \times 10^{-2}$ M^{-1} (from eq 6) for eq 27–30,

$$OH + H^+ + SO_4^{2-} = SO_4^- + H_2O \quad (27)$$

$$H_2O = OH + H^+ + e^- \quad (28)$$

$$S_2O_8^{2-} + 2e^- = 2SO_4^{2-} \quad (29)$$

$$SO_4^- + SO_4^{2-} = SO_4^-|SO_4^{2-} \quad (30)$$

respectively. It will be seen that the experimental points conform reasonably well to the model for a value of $\Delta G^*(0)$ somewhat larger than 20 kcal/mol.

The ruthenium ammine complexes studied in the present work have different charges and different self-exchange rates. The charges affect the values of k_{12}, k_{21}, and k_{30}, and the self-exchange rates are implied in $\Delta G^*(0)$ which is (eq 31) the average of the

$$\Delta G^*(0) = (\Delta G_{11}^* + \Delta G_{22}^*)/2 \quad (31)$$

intrinsic barriers for the reacting couples. Therefore, before the rate constants for the ammine complexes can be plotted in the same figure as the iron, ruthenium, and osmium polypyridine complexes, the observed values must be corrected for charge and self-exchange rate differences. This was accomplished in an approximate manner by utilizing eq 32, where $(k_{11}^{1/2}w_{12})_a$ includes

$$k_{cor} = k_{obsd}(k_{11}^{1/2}w_{12})_b/(k_{11}^{1/2}w_{12})_a \quad (32)$$

the rate constant for self-exchange and work term for the ruthenium complex to be corrected and the factor $(k_{11}^{1/2}w_{12})_b$ includes the corresponding parameters for the polypyridine complexes. Considering the substantial (and approximate) corrections for electrostatic and self-exchange effects, it will be seen that the resulting points (circles) conform reasonably well[28] to the model with a $\Delta G^*(0)$ of ~20 kcal/mol. Points for $Co(bpy)_3^{2+}$ (filled square) and Fe^{2+} (circle), corrected according to eq 32, are also included in Figure 4. It will be seen that the point for $Co(bpy)_3^{3+}$ falls nicely in line with the other polypyridine complexes, but the point for Fe^{2+} is considerably higher. Presumably the Fe^{2+}–$S_2O_8^{2-}$ reaction, just like the analogous Cr^{2+}–$S_2O_8^{2-}$ reaction,[29] proceeds via a more efficient inner-sphere mechanism, and the associated rate constant falls above the line defined by the remaining outer-sphere reactions.

A fit of the measurements for the polypyridine complexes to eq 25 and 26 yields a value of $\Delta G^*(0)$ of about 22 kcal/mol. From eq 31, taking ΔG_{11}^* for the polypyridine complexes as ~4 kcal/mol, we obtain $\Delta G_{22}^* \sim 40$ kcal for the self-exchange reaction of the $S_2O_8^{2-}/SO_4^-\cdot SO_4^{2-}$ couple. This corresponds to a rate constant of $\sim 10^{-18}$ M^{-1} s^{-1}. Such a high barrier does not seem unreasonable for a self-exchange reaction that involves as substantial a molecular reorganization as the breaking of a bond. Interestingly, the homogeneous reductions of aliphatic halides by electrogenerated anion radicals have been analyzed according to the Marcus activation free energy–standard free energy relationship on the basis of a reductive cleavage process ($RX + e^- = R^\cdot + X^-$).[19-21] Good correlations were obtained with activation free energies for the self-exchange reactions of the couples $RX/R^\cdot X^-$ (R = *n*-butyl, sec-butyl, *tert*-butyl; X = Cl, Br, I)[20,21] in the range 28–41 kcal/mol.

Scheme IV

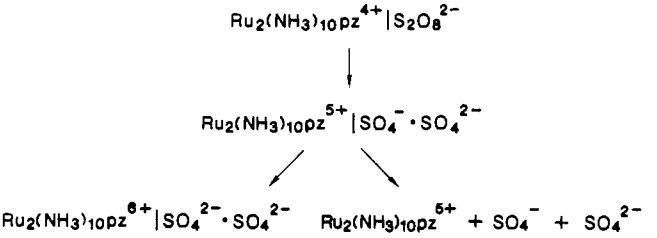

Finally, we address the question of one- vs. two-electron oxidation of $Ru_2(NH_3)_{10}pz^{4+}$. The experimental results demonstrate that ~80% of the $Ru_2(NH_3)_{10}pz^{4+}$–$S_2O_8^{2-}$ reaction proceeds by the two-electron mechanism and yields directly $Ru_2(NH_3)_{10}pz^{6+}$. However, we do not believe that this pathway represents a genuine two-electron transfer mechanism, e.g., that the two electrons are transferred "simultaneously". We favor a sequence of two one-electron transfers, Scheme IV. The reactant ion pair undergoes a one-electron reaction to yield the ion pair $Ru_2(NH_3)_{10}^{5+}|SO_4^-\cdot SO_4^{2-}$. Now there is competition between the second electron transfer to yield the 80% observed kinetic product $Ru_2(NH_3)_{10}pz^{6+}$ and ion-pair separation to yield the one-electron product $Ru_2(NH_3)_{10}pz^{5+}$. The rate of ion-pair separation is estimated as ~10^9 s^{-1}, and therefore the rate of internal electron transfer in $Ru_2(NH_3)_{10}pz^{5+}|SO_4^-\cdot SO_4^{2-}$ must be on the order of ~10^{10} s^{-1}, a not unreasonable value for a highly exoergonic reaction (E° for SO_4^-/SO_4^{2-} is ~2.6 V) with a low intrinsic barrier.[30]

Acknowledgment. This work was supported on National Science Foundation Grant CHE-8502079.

Registry No. $Ru(NH_3)_5pz^{2+}$, 19471-65-9; $Ru(NH_3)_4bpy^{2+}$, 54194-87-5; $Ru(NH_3)_5pzMe^{3+}$, 48135-76-8; $Ru_2(NH_3)_{10}pz^{5+}$, 35599-57-6; $RuRh(NH_3)_{10}pz^{5+}$, 48170-08-7; $Ru_2(NH_3)_{10}pz^{4+}$, 26253-76-9; $S_2O_8^{2-}$, 15092-81-6.

(28) However, if the corrections are taken at face value, it appears that the slope of log k_{cor} vs ΔG_{23}° for the ruthenium ammine complexes is somewhat smaller than log k_{obsd} vs ΔG_{23}° for the polypyridine complexes. The mechanistic significance of this difference, if real, is not apparent. It may be that, for the ammine complexes, the bond cleavage contributes more to the activation process and thus the rate is less sensitive to the thermodynamics of the redox process.

(29) Pennington, D. E.; Haim, A. *J. Am. Chem. Soc.* **1968**, *90*, 3700.

(30) Unfortunately, the self-exchange rate for the SO_4^-/SO_4^{2-} couple is unknown. However, low inner-sphere and outer-sphere reorganization energies are expected for the electron exchange between the structurally similar and relatively low-charged species SO_4^- and SO_4^{2-}.